Outdoor evaluation of total cross-tied Si module under driving conditions

Solar Energy Materials & Solar Cells 274 (2024) 112989

Contents lists available at ScienceDirect

Solar Energy Materials and Solar Cells

journal homepage: www.elsevier.com/locate/solmat

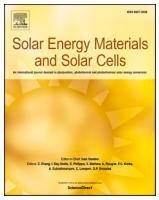

Outdoor evaluation of total cross-tied Si module under driving conditions

Yasuyuki Ota [a,b,*], Keiya Tamada [b], Kyotaro Nakamura [c], Masafumi Yamaguchi [c], Yoshio Ohshita [c], Kenji Araki [a], Kensuke Nishioka [a,b]

[a] GX Research Center, University of Miyazaki, 1-1, Gakuen Kibanadai-Nishi, Miyazaki, 889-2192, Japan
[b] Graduate School of Engineering, University of Miyazaki, Miyazaki, Japan
[c] Toyota Technological Institute, Nagoya, Japan

ARTICLE INFO

Keywords:
Vehicle-integrated photovoltaic
Total cross-tied configuration
Partial shading
Dynamic shading
Maximum power point tracking

ABSTRACT

This paper presents the fabrication and evaluation of a total cross-tied (TCT) Si module designed to mitigate the partial shading effect, which is known to reduce the output performance of vehicle-integrated photovoltaic (VIPV) modules. The TCT module, consisting of 27 Si solar cells interconnected both vertically and horizontally, demonstrated an 18.8 % decrease in output power when one cell was shaded. In contrast, the output of the series-parallel (SP) Si module decreased by 31.6 % under the same shading condition. Comparative analysis of the output performances of TCT, SP, and single-string commercial modules under three driving conditions revealed that increasing the number of strings helped alleviate the impact of partial shading. Notably, the TCT module configuration showed a positive impact on mitigating the partial shading effect.

1. Introduction

Reducing greenhouse gas emissions is a global challenge. In 2021, industry and lifestyle activities emitted 1170 million tons of carbon dioxide equivalent [1]. Carbon dioxide accounted for the majority of Japan's greenhouse gas emissions at 1064 million tons, with approximately 17.4 % originating from the transportation sector. Traditional transportation, such as automobiles, relies on fossil fuels and internal combustion engines, resulting in carbon dioxide emissions. Electric vehicles (EVs) offer significant potential to reduce these emissions compared to traditional internal combustion engine vehicles [2]. Additionally, charging EVs with electricity from renewable sources like solar, wind, and hydro can further minimize their overall carbon footprint, enhancing their environmental friendliness. Among renewable energy sources, solar energy, harnessed through photovoltaic (PV) systems, plays a pivotal role globally. Utilizing PV systems to supply electricity to EVs is crucial for reducing carbon dioxide emissions. PV charging stations can effectively provide electricity generated by PV systems to EVs [3–5].

Conversely, PV modules directly mounted onto vehicles or vehicle-integrated photovoltaic (VIPV) systems are attractive alternatives [6]. Masuda et al. [7] investigated PV panels mounted on a car body and measured their energy generation. They found that vehicles driving less than 30 km/day on average, constituting 70 % of Japanese passenger vehicles, could rely on solar energy to charge their batteries without grid dependence, potentially reducing greenhouse gas emissions by 8 %. Toyota Motor Corporation developed a PV-powered vehicle based on the Prius plug-in hybrid vehicle (PHV) [8]. Equipped with InGaP/GaAs/InGaAs triple-junction solar cells [9] providing an output of 860 W and an irradiance meter, Toyota estimated driving distance using collected irradiance data. However, the calculated driving distance was shorter than predicted, possibly due to partial shading, the 3-dimensional PV module surface, and module orientation.

VIPV systems present unique challenges compared to conventional flat PV systems, particularly due to the curved nature of vehicle surfaces. These curved surfaces often result in self-shading of the panels [10,11], leading to non-uniform irradiance distribution. While driving or parked, VIPV systems are further shaded by various objects such as buildings, trees, poles, and distant mountains. This partial shading reduces PV output performance [12,13] and may lead to hot spots [14]. We assessed the impact of partial shading, including dynamic shading [15]. Shading probability was influenced by the height of shading objects, and a reduced sky view factor increased shading probability. Partial shading also decreased PV output. Adjusting the string configuration was crucial to mitigate the impact of partial shading.

PV systems employ various configurations, including series-parallel (SP), total-cross-tied (TCT), Honey-comb (HC), and bridge-linked (BL), to mitigate partial shading losses [16]. The SP configuration, where

* Corresponding author. GX Research Center, University of Miyazaki, 1-1, Gakuen Kibanadai-Nishi, Miyazaki, 889-2192, Japan.
E-mail address: y-ota@cc.miyazaki-u.ac.jp (Y. Ota).

https://doi.org/10.1016/j.solmat.2024.112989
Received 30 April 2024; Received in revised form 7 June 2024; Accepted 8 June 2024
Available online 12 June 2024

modules are connected in series and then in parallel, is the fundamental setup in conventional systems. The TCT configuration connects ties across rows of modules, based on the SP configuration, with output power equal to that of the SP configuration. The BL configuration resembles a bridge rectifier connection. The HC configuration offers advantages over TCT and BL configurations [17,18]. Mohammadnejad et al. [19] demonstrated that the TCT configuration outperformed other configurations under various partial shading conditions using a single-diode solar cell model simulation. The TCT configuration offers advantages as a module assembly. Suriya Kala et al. [20] compared a 16-solar cell series-connected PV module with 2 bypass diodes to a 4 × 4 TC T module with 4 bypass diodes. Solar cells were connected in a TCT configuration to maintain higher power output under partial shading conditions.

In this study, we manufactured the TCT configuration PV module and assessed its output under partial shading conditions through outdoor measurements. Furthermore, we investigated the advantage of mounting the TCT configuration PV module on the car roof in mitigating partial and dynamic shading during actual driving.

2. Partial shading tests for TCT mini module

Previously, we estimated the impact of partial shading on power loss in solar cell modules using SPICE software and conducted partial shading tests on mini-modules consisting of 6 × 6 Si hetero-junction (SHJ) solar cells measuring 2 cm × 2 cm, fabricated by Toyota Technological Institute [21]. Fig. 1 illustrates a series-parallel connection (SP) solar cell module with 6 series and 6 parallel connections, alongside a total cross-tied (TCT) solar cell module comprising 36 solar cells. The TCT module, with 6 series × 6 parallel connections, links all nodes of rows to minimize power loss under partial shading. The simulated and experimental power output of the TCT module under partial shading exhibited a strong correlation, validating the evaluation procedure for partial shading of solar cell modules. Additionally, the simulated output power of the TCT module with bypass diodes demonstrated further reduction in partial shading effects.

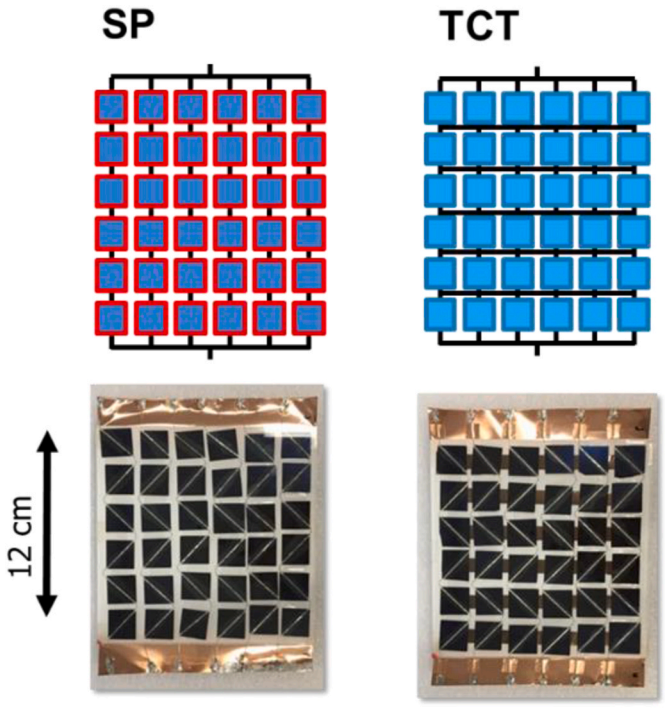

Fig. 1. SP solar cell module with 6 series and 6 parallel connections; TCT solar cell module connecting all nodes of rows in SP configuration.

3. Experimental procedure

The TCT module comprised 27 Si solar cells measuring 156 mm × 52 mm. Each solar cell was connected both vertically and horizontally. Additionally, we fabricated the SP module, comprising 9 series and 3 parallel Si solar cells within the same 156 mm × 52 mm area. Both modules underwent IV characteristics and EL image measurements under indoor conditions. Outdoor IV characteristic measurements were conducted using an IV tracer (MP-160, EKO Instruments CO., LTD.) under static partial shading with varied patterns. However, under dynamic partial shading during driving conditions, IV measurements could not accurately track module output characteristics. To measure the output of both modules, we applied an electric load with maximum power point tracking (ECL02401, Nippon Kernel System CO., LTD.). Fig. 2 illustrates the experimental setup on the car roof, where the PV modules were installed alongside a pyranometer (SR20, Hukseflux Thermal Sensors B·V.). The setup also included a commercial PV module (NQ-143, SHARP Corporation). Output measurements were obtained under maximum power point (P_m) conditions. The electronic load was controlled using the MPPT system, sweeping from open-circuit voltage to zero every minute and searching for the maximum power point every second. Operating currents and voltages at the maximum power point were recorded by a data logger every 0.1 s. Additionally, car roof irradiances were recorded using the same procedure for currents and voltages.

We introduced the sky view factor (SVF) [22] to assess the shading objects around the passenger vehicle during driving. The SVF is defined as follows:

$$SVF = 1 - \frac{\int_{0^\circ}^{360^\circ}\int_{0^\circ}^{90^\circ}\theta(\varphi)d\theta d\varphi}{90^\circ \bullet 360^\circ} \quad (1)$$

where $\theta(\varphi)$ is the profile line of shading objects, as shown in Fig. 3. To capture the shading object profile, we utilized a spherical camera (WV–S4550L, Panasonic Corporation). Typically, this camera is positioned high, facing downwards to capture a wide range of surrounding images through a window. However, in this experiment, we inverted its position to record the sky from below. Fig. 4 (a) displays a sample of the spherical camera image, with y + indicating the direction of travel. Semantic segmentation processing was applied to the image to identify the sky and structures, as depicted in Fig. 4 (b). Subsequently, the SVF was calculated based on the sky area. During the experiment, this procedure was applied to the video footage, allowing for continuous SVF calculation.

We assessed the output performances of the modules during parking, driving in an open-air zone, and driving in a building zone. The open-air zone spanned 8.5 km, with the vehicle equipped with PV modules traveling in a single direction. In the building zone, the vehicle completed three loops of the course. Table 1 provides a summary of the driving and parking conditions.

Fig. 2. Experimental setup on the car roof, featuring SP and TCT PV modules installed horizontally alongside a pyranometer. The system also incorporates a commercial PV module.

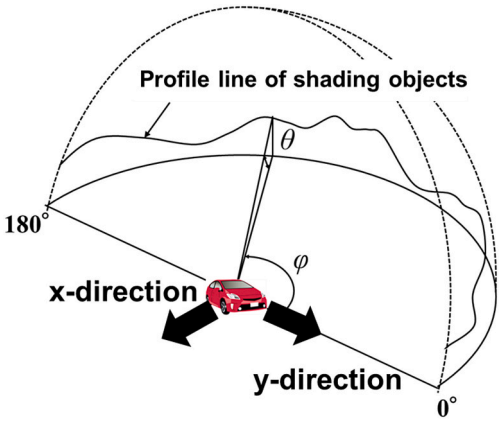

Fig. 3. Definition of grazing angle (θ) and orientation angle (φ).

4. Results and discussion

4.1. Indoor measurements and static partial shading conditions

Fig. 5 displays the photograph and EL image of the SP and TCT modules, respectively. Table 2 provides a summary of the IV characteristics obtained from indoor measurements. Both modules exhibit satisfactory output performances. Fig. 6 illustrates the normalized conversion efficiency of both modules as a function of the number of shaded solar cells under static partial shading conditions. The shaded solar cells increase along the x-direction. These measurements were conducted outdoors. As the number of shaded solar cells increased, the conversion efficiency decreased. However, the decrease in efficiency for the TCT module was less pronounced compared to the conventional Si module. Specifically, the output power of the TCT Si module decreased by 18.8 % when one Si solar cell was shaded, whereas the output of the conventional Si module decreased by 31.6 % under the same shading condition. This indicates that the TCT module mitigates output power degradation resulting from partial shading.

4.2. Evaluation of the module while driving

In section 4.1, we assessed the STC conditions for the PV modules and the static partial shading effects on outdoor module output. The PV module, previously mounted on the car body, was relocated onto the road. We previously measured the output of a single-string PV module installed on the car roof and identified the impact of shading objects such as buildings, infrastructure electric wires, and houses [12]. Consequently, dynamic partial shading influenced the module's output. In this study, we compared the output performances of TCT, SP, and single-string commercial modules under three conditions: parking, driving in an open zone, and driving in a buildings zone.

Fig. 7 depicts the SVF as a function of driving time under the building

Table 1
Summary of driving and parking conditions, indicating parking and driving times during the experimental period, along with the average sun altitude.

	Experimental period (min)	Distance (km)	Ave. SVF	Ave. Sun altitude (deg)
Parking	60	–	0.85	31.6
Driving – open air	9	8.5	0.87	34.2
Driving - buildings	32	9.6	0.61	35.0

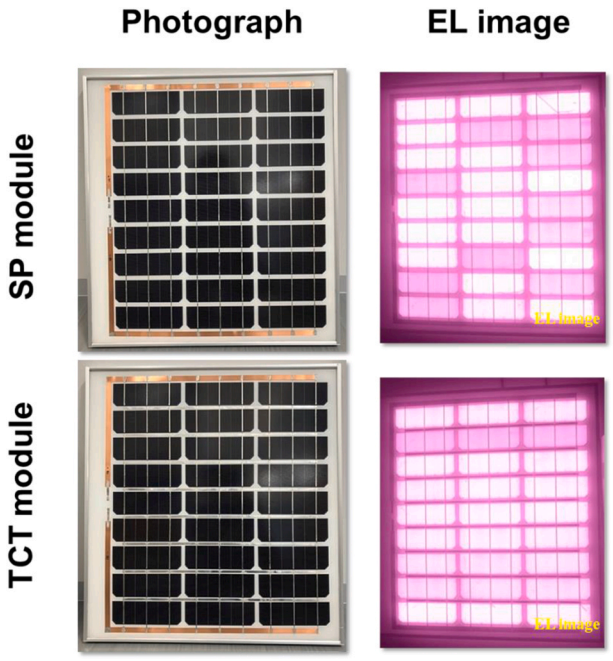

Fig. 5. Photograph and EL image of the SP and TCT modules.

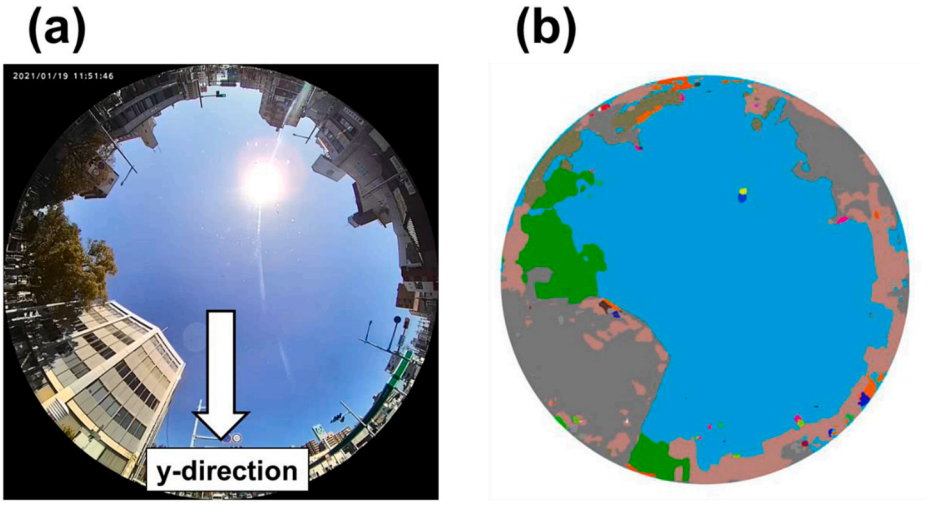

Fig. 4. (a) Sample image captured by the spherical camera. (b) Result of semantic segmentation processing.

Table 2
Summary of IV characteristics in indoor measurements.

	I_{sc} (A)	V_{oc} (V)	FF	P_{max} (W)	η_{mod} (%)	η_{cell} (%)
SP module	10.2	6.12	0.828	51.7	14.2	23.4
TCT module	10.0	6.10	0.836	51.0	14.1	23.1

zone. The distribution of buildings varied with time (traveling position), resulting in a non-constant SVF while driving. The minimum SVF recorded was 0.30, indicating that buildings obscured 70 % of the sky, while the average SVF during the building zone experiment was 0.61. Conversely, the average SVF during the open zone was 0.87. In parking, the SVF remained constant at 0.85. Fig. 8 displays typical spherical camera images of each zone. The SVF influenced the shading probability, with a higher likelihood of shading occurring with decreasing sky view factor [15]. Hence, partial shading was more prevalent in the building zone. A high shading probability indicated an increased likelihood of shading the sun (direct irradiance), while the SVF contributed to a portion of the diffused irradiance.

Fig. 9 shows the performance ratio (*PR*) variation during the driving in the building zone. The *PR* values were re-sampled in 5-s intervals as an average and normalized by the parking condition. Table 3 summarizes the *PR* of each module during the experimental period. The duration of open zone driving was shorter compared to other conditions due to smooth traffic flow. The *PR* values are presented as a percentage of the *PR* values under parking conditions. Under building zone driving, the *PR* value of the one-string module decreased to 95.6 % due to partial shading. However, increasing the number of strings mitigated the impact of partial shading, as demonstrated by the SP module. The *PR* value of the TCT module decreased to 97.8 % under building zone driving, indicating a positive impact of the module configuration, such as the TCT module, on partial shading. Driving also affected module temperature, influencing performance. The performance of the PV module under driving in Table 3 included the temperature effect. The module configuration, including aperture area, EVA thickness, and buck sheet material, remained consistent between the TCT and SP modules while differing from the configuration of the conventional commercial PV module. Consequently, module temperatures were not anticipated to be significantly different between the TCT module and the SP module.

5. Conclusion

This study involved manufacturing and evaluating the TCT configuration PV module under partial shading conditions. Our findings indicate that in static partial shading scenarios, the TCT module exhibited a lesser decline in conversion efficiency compared to conventional Si modules as the number of shaded solar cells increased. This suggests that the TCT module is effective in reducing output power degradation resulting from partial shading. Furthermore, through a comparison of output performances among TCT, SP, and single-string commercial modules under various conditions, we observed that increasing the number of strings helped mitigate the impact of partial shading. Notably, the TCT module configuration demonstrated a positive effect in alleviating the effects of partial shading.

Funding sources

This work received support from the New Energy and Industrial Technology Development Organization (NEDO), Japan (Project number: JPNP20015).

CRediT authorship contribution statement

Yasuyuki Ota: Writing – review & editing, Writing – original draft, Visualization, Supervision, Data curation. **Keiya Tamada:** Investigation. **Kyotaro Nakamura:** Writing – review & editing, Visualization, Resources, Formal analysis. **Masafumi Yamaguchi:** Formal analysis. **Yoshio Ohshita:** Funding acquisition. **Kenji Araki:** Methodology. **Kensuke Nishioka:** Project administration, Funding acquisition.

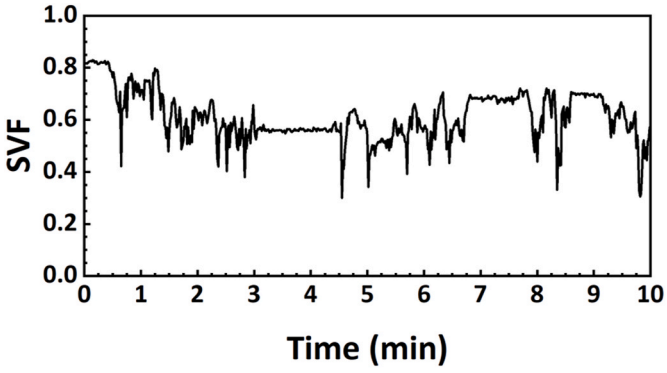

Fig. 7. Sky view factor (SVF) plotted against driving time in the building zone.

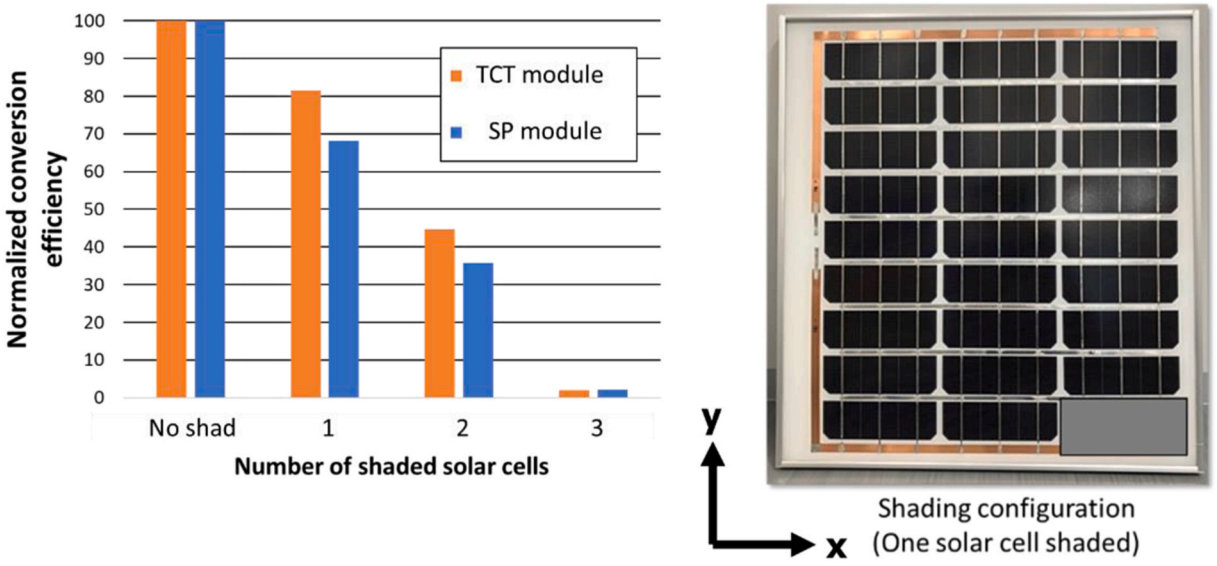

Fig. 6. Normalized conversion efficiency of both modules plotted against the number of shaded solar cells under static partial shading conditions.

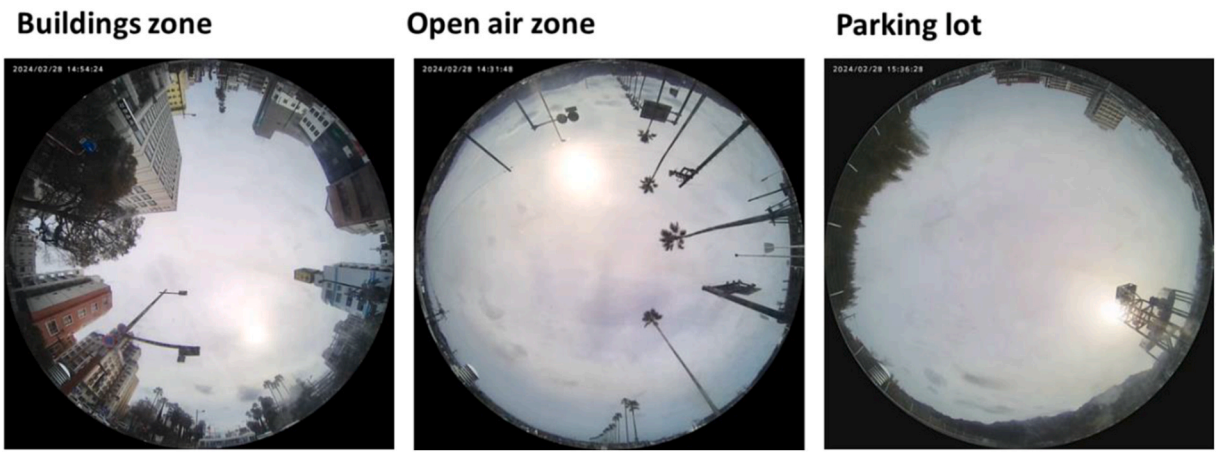

Fig. 8. Typical spherical camera images of each zone.

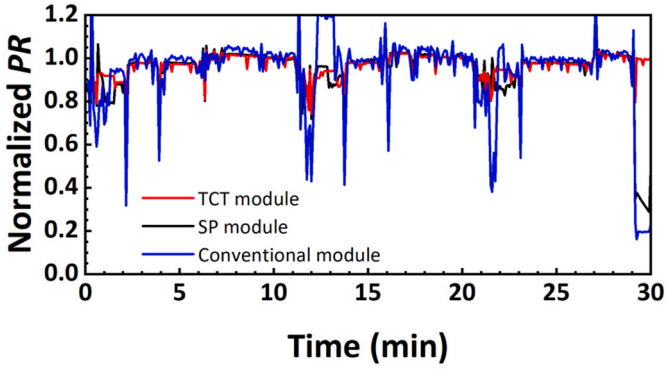

Fig. 9. *PR* variation during the driving in the building zone.

Table 3
Summary of performance ratio (*PR*) values for each module during the experimental period, normalized by the parking condition.

	TCT module	SP module (3 strings)	Conventional (1 string)
Parking	1.000	1.000	1.000
Driving – open air	0.977	0.986	1.001
Driving - buildings	0.978	0.962	0.956

Declaration of competing interest

The authors declare that they have no known competing financial interests or personal relationships that could have appeared to influence the work reported in this paper.

References

[1] National Greenhouse Gas Inventory Report of japan, Ministry of the Environment, Japan. Greenhouse Gas Inventory Office of Japan (GIO), CGER, NIES.
[2] C. Breyer, S. Khalili, D. Bogdanov, Solar photovoltaic capacity demand for a sustainable transport sector to fulfil the Paris Agreement by 2050, Prog. Photovoltaics. 27 (2019) 978–989.
[3] D. Wang, M. Sechilariu, F. Locment, PV-powered charging station for electric vehicles: power Management with integrated V2G, Appl. Sci. 10 (2020) 6500.
[4] Q. Dai, J. Liu, Q. Wei, Optimal photovoltaic/battery energy storage/electric vehicle charging station design based on multi-agent particle swarm optimization algorithm, Sustainability 11 (2019) 1973.
[5] A. Borchers, T. Pieler, Programming pluripotent precursor cells derived from Xenopus embryos to generate specific tissues and organs, Genes 1 (2010) 413–426.
[6] C. Thiel, A. Gracia Amillo, A. Tansini, A. Tsakalidis, G. Fontaras, E. Dunlop, N. Taylor, A. Jäger-Waldau, K. Araki, K. Nishioka, Y. Ota, M. Yamaguchi, Impact of climatic conditions on prospects for integrated photovoltaics in electric vehicles, Renew. Sustain. Energy Rev. 158 (2022) 112109.
[7] T. Masuda, K. Araki, K. Okumura, S. Urabe, Y. Kudo, K. Kimura, T. Nakado, A. Sato, M. Yamaguchi, Static concentrator photovoltaics for automotive applications, Sol. Energy 146 (2017) 523–531.
[8] M. Yamaguchi, T. Masuda, K. Araki, D. Sato, K.H. Lee, N. Kojima, T. Takamoto, K. Okumura, A. Satou, K. Yamada, T. Nakado, Y. Zushi, Y. Ohshita, M. Yamazaki, Development of high-efficiency and low-cost solar cells for PV-powered vehicles application, Prog. Photovoltaics. 29 (2020) 684–693.
[9] Y. Ota, K. Ueda, T. Takamoto, K. Nishioka, Output evaluation of a world's highest efficiency flat sub module with InGaP/GaAs/InGaAs inverted triple-junction solar cell under outdoor operation, Jpn. J. Appl. Phys. 57 (2018) 08RD08.
[10] Y. Ota, K. Araki, A. Nagaoka, K. Nishioka, Facilitating vehicle-integrated photovoltaics by considering the radius of curvature of the roof surface for solar cell coverage, Cleaner. Engineer.Techn. 7 (2022) 100446.
[11] Y. Ota, K. Araki, A. Nagaoka, K. Nishioka, Curve correction of vehicle-integrated photovoltaics using statistics on commercial car bodies, Prog. Photovoltaics. 30 (2022) 152–163.
[12] Y. Ota, K. Araki, A. Nagaoka, K. Nishioka, Evaluating the output of a car-mounted photovoltaic module under driving conditions, IEEE J. Photovoltaics 11 (2021) 1299–1304.
[13] P. Hoth, L. Heide, A. Grahle, D. Göhlich, Vehicle-integrated photovoltaics—a case study for berlin, World Electric Veh. J. 15 (2024) 113.
[14] M. Heinrich, C. Kutter, F. Basler, M. Mittag, L.E. Alanis, D. Eberlein, A. Schmid, C. Reise, T. Kroyer, D.-H. Neuhaus, H. Wirth, Potential and Challenges of Vehicle Integrated Photovoltaics for Passenger Cars, EU PVSEC 2020, 2020, pp. 1695–1700.
[15] K. Araki, Y. Ota, A. Nagaoka, K. Nishioka, 3D solar irradiance model for non-uniform shading environments using shading (aperture) matrix enhanced by local coordinate system, Energies 16 (2023).
[16] R. Ramaprabha, B.L. Mathur, A comprehensive review and analysis of solar photovoltaic array configurations under partial shaded conditions, Int. J. Photoenergy 2012 (2012) 1–16.
[17] Y.-J. Wang, P.-C. Hsu, Analysis of partially shaded PV modules using piecewise linear parallel branches model, World Acad.Sci. Engineer. Techn. 60 (2009) 783–789.
[18] Y.-J. Wang, P.-C. Hsu, An investigation on partial shading of PV modules with different connection configurations of PV cells, Energy 36 (2011) 3069–3078.
[19] S. Mohammadnejad, A. Khalafi, S.M. Ahmadi, Mathematical analysis of total-cross-tied photovoltaic array under partial shading condition and its comparison with other configurations, Sol. Energy 133 (2016) 501–511.
[20] S. Suriya kala, D. Prince winston, M. Pravin, G. Sakthivel, Maximum power enhancement in solar PV modules through modified TCT interconnection method, Sustain. Energy Technol. Assessments 60 (2023) 103462.
[21] K. Nakamura, C. Okamoto, R. Ozaki, Y. Ohshita, M. Yamaguchi, Proposal of Solar Cell Modules for Reducing Partial Shading Loss, EU PVSEC 2023, 2023.
[22] M. Dirksen, R.J. Ronda, N.E. Theeuwes, G.A. Pagani, Sky view factor calculations and its application in urban heat island studies, Urban Clim. 30 (2019) 100498.